

# Relative abundances and enantiomerization energy of the chiral $\text{Cu}_{13}$ cluster at finite temperature

César Castillo-Quevedo,<sup>1</sup> Carlos Emiliano Buelna-García,<sup>2,3</sup> Edgar Paredes-Sotelo,<sup>2</sup> Eduardo Robles-Chaparro,<sup>4</sup> Gerardo Martínez-Guajardo,<sup>5</sup> Jesús Manuel Quiroz-Castillo,<sup>2</sup> Aned de-Leon-Flores,<sup>4</sup> Tulio Gaxiola,<sup>6</sup> Santos Jesus Castillo,<sup>7</sup> Alejandro Vásquez-Espinal,<sup>8</sup> and Jose Luis Cabellos<sup>7,\*</sup>

<sup>1</sup>*Departamento de Fundamentos del Conocimiento,  
Centro Universitario del Norte, Universidad de Guadalajara,  
Carretera Federal No. 23, Km. 191, C.P. 46200, Colotlán, Jalisco, México*

<sup>2</sup>*Departamento de Investigación en Polímeros y Materiales,  
Edificio 3G, Universidad de Sonora. Hermosillo, Sonora, México*

<sup>3</sup>*Organización Científica y Tecnológica del Desierto, Hermosillo 83150, Sonora, México*

<sup>4</sup>*Departamento de Ciencias Químico Biológicas, Edificio 5A, Universidad de Sonora. Hermosillo, Sonora, México*

<sup>5</sup>*Unidad Académica de Ciencias Químicas, Área de Ciencias de la Salud,  
Universidad Autónoma de Zacatecas, Km. 6 carretera Zacatecas-Guadalajara s/n,  
Ejido La Escondida C. P. 98160, Zacatecas, Zac.*

<sup>6</sup>*Facultad de Ciencias Físico-Matemáticas de la Universidad Autónoma de Sinaloa, 80010, Sinaloa, México*

<sup>7</sup>*Departamento de Investigación en Física, Universidad de Sonora,  
Blvd. Luis Encinas y Rosales S/N, 83000 Hermosillo, Sonora, México*

<sup>8</sup>*Computational and Theoretical Chemistry Group Departamento de Ciencias Químicas,  
Facultad de Ciencias Exactas, Universidad Andres Bello, Republica 498, Santiago, Chile*  
(Dated: September 10, 2021)

This study reports the lowest energy structure of bare  $\text{Cu}_{13}$  nanoclusters as a pair of enantiomers for temperatures ranging from 20 to 1200 K. Moreover, we compute the enantiomerization energy for the interconversion from  $\mathcal{M}$  to  $\mathcal{P}$  structures in the chiral putative global minimum for temperatures ranging from 20 to 1300 K. Additionally, employing statistical thermodynamics and nanothermodynamics, we compute the Boltzmann Probability for each particular isomer as a function of temperature. To achieve that, we explore the free energy surface of the  $\text{Cu}_{13}$  cluster, employing a genetic algorithm coupled with density functional theory and statistical thermodynamics. Moreover, we discuss the energetic ordering of structures computed at the DFT level and compared to high level DLPNO-CCSD(T1) reference energies, and we present chemical bonding analysis using the AdNDP method in the chiral putative global minimum. Based on the computed relative abundances, our results show that the chiral putative global minimum strongly dominates for temperatures ranging from 20 to 1100 K.

PACS numbers: 61.46.-w,65.40.gd,65.65.80.-g,67.25.bd,71.15.-m,71.15.Mb,74.20.Pq,74.25.Bt,74.25.Gz,74.25.Kc

Keywords: Copper clusters,  $\text{Cu}_{13}$ , chiral, density functional theory, temperature, Boltzmann probabilities, Gibbs free energy, entropy, enthalpy, nanothermodynamics, thermochemistry, statistical thermodynamics, genetic algorithm, DLPNO-CCSD(), Adaptive Natural Density Partitioning method (AdNDP), Enantiomerization energy, DFT, Global minimum

## I. INTRODUCTION

Transition-metal (TM) nanoclusters have been widely studied due to their potential applications in catalysis<sup>1-3</sup>, photoluminescence<sup>4</sup>, photonics<sup>5</sup>, magnetism<sup>4</sup>, chirality<sup>6</sup>, and the design of new materials<sup>7,8</sup>. Cu is a 3d TM with several oxidation states<sup>9,10</sup>, which explains its reactivity and confers many interesting physical and chemical properties<sup>9,10</sup>. Moreover, the high boiling point of Cu makes it compatible with high-temperature chemical reactions. Clusters are aggregates of atoms at the nanoscale size, which exhibit unusual physicochemical properties<sup>11</sup>. Cu clusters are particularly fascinating due to their applications in catalysis<sup>10</sup>, light-emitting devices<sup>12</sup>, and nanotechnology<sup>13</sup>, despite presenting some challenges such as their easy oxidation<sup>13</sup>. The most stable structure of small Cu clusters has been investigated by density functional theory (DFT) studies<sup>14-17</sup> and considering the

*Jahn-Teller effect*<sup>18</sup>. In the early 2000s, Poater et al.<sup>19</sup> characterized neutral copper clusters ( $\text{Cu}_n$   $n = 1-9$ ) using computed chemical reactivity descriptors within the DFT framework. Later, atomic structures and reactivity descriptors of  $\text{Cu}_n\text{CO}$  ( $n = 1,9$ ) were computed and discussed<sup>19</sup>. Calaminici et al. reported the structure of neutral and anionic  $\text{Cu}_9$  clusters, employing DFT<sup>20</sup>. Moreover, in previous combined theoretical-experimental studies, the computed removal energies were compared with the measured photoelectron spectra in anionic  $\text{Cu}_n$  ( $n = 9,20$ ) clusters<sup>21</sup>, and later, the optical absorption of small Cu clusters was presented<sup>22</sup>. Based on their geometry and electronic structure, atomic clusters could be characterized by magic numbers<sup>1,23-25</sup> that form highly symmetric structures; for example, icosahedron (ICO) and cuboctahedron (CUB) shapes<sup>1</sup>. From the geometrical point of view, the first magic number that appears is 13. Experimental studies have found magic  $\text{TM}_{13}$  clusters for Fe and Ti, amongst others<sup>1,26</sup>. Previous theo-

retical studies based on the empirical potential of  $\text{Cu}_{13}$  clusters showed that the low-energy structures were the icosahedron and the cuboctahedron<sup>27</sup>; those structures consist of a central atom surrounded by 12 Cu atoms. In contrast, Guvelioglu et al.<sup>28</sup>, within the framework of DFT, found that the lowest energy structure of  $\text{Cu}_{13}$  is the double-layered structure, and in the same year Itoh et al.<sup>29</sup> reported a similar double-layer structure as the putative global minimum. Yang et al. explored the structural evolution of  $\text{Cu}_n$  ( $n = 8-20$ ) anions and found plate-like structures<sup>30</sup>. Later, larger  $\text{Cu}_n$  ( $n = 20-30$ ) clusters were investigated, and it was found that the structures are based on a 13-atom icosahedral core<sup>31</sup>. In the previous studies,  $\text{Cu}_{13}$  was investigated because it was found to have an icosahedral structure that has a high percentage of edge and corner sites and high-index facets, resulting in increased catalytic activities<sup>32-34</sup>. In most cases, low-energy Cu clusters have preferentially lower symmetry structures<sup>35</sup>, although some present distorted structures<sup>35,36</sup>. Although there are many studies on Cu clusters, the chirality of  $\text{Cu}_{13}$  clusters has not been discussed. In general, chirality plays a decisive role in biological activity and life processes.<sup>37</sup> Remarkably, chiral nanoclusters have attracted attention because they have applications in chiral materials with novel properties<sup>38-40</sup>. Recently, theoretical studies on beryllium boron cluster  $\text{Be}_4\text{B}_8$  at the DLPNO-CCSD(T1) theoretical level found chiral structures as the lowest energy structures<sup>40</sup>. Previous theoretical studies on PtPd co-doped silicon clusters reported chiral and fluxional low-energy structures<sup>41</sup>. Recently, Kong et al. reported propeller-like chiral AIE copper (I) clusters with exciting properties<sup>42</sup>. However, clusters' properties depend on their putative global minimum and low-energy structures, considering achiral and chiral structures. Hence, we need to know the distributions of isomers at different temperatures<sup>40,43,44</sup>. The lowest- and low-energy geometries, composition, and temperature of the ensemble determine all the properties of a cluster at temperature  $T$ <sup>43-45</sup>, i.e., its electronic, structural, thermodynamics, vibrational, and optical properties, as well as its chemical reactivity. Moreover, the atomic structure is the first level at which it is possible to manipulate the macroscopic properties of a cluster<sup>1</sup>.

In this study, intending to elucidate the lowest- and the low-energy structures of neutral  $\text{Cu}_{13}$  clusters at finite temperature, we explored their free energy surface by employing a genetic algorithm coupled to DFT, statistical thermodynamics and nanothermodynamics. We computed the probability of occurrence of each particular isomer, employing Boltzmann probabilities for temperatures ranging from 20 to 1500 K. Our findings show that the putative global minimum is a chiral structure at room temperature. Moreover, we computed the transition state (TS), i.e., the enantiomerization energy for temperatures ranging from 20 to 1300 K, for interconversion of a pair of enantiomers (Plus,  $\mathcal{P}$ , and Minus,  $\mathcal{M}$ ). Our computations showed that enantiomerization

barriers led to persistently chiral structures and enabled the complete separation of enantiomers at room temperature<sup>40,46</sup>. The remainder of the manuscript is organized as follows. Section 2 provides the computational details and a brief overview of the theory and the algorithms used. The results and discussion are presented in Section 3. We discuss the low-energy structures, the effect of the DFT functionals on the energetic ordering of isomers and comparison to DLPNO-CCSD(T1)<sup>47</sup> reference energies; T1 diagnostic is presented. The effect of the symmetry number on the Gibbs free energy and on the thermal populations at temperature  $T$ ; and the origin of the slight 0.41 kcal/mol energy differences are investigated. We analyze the interconversion energy barrier between  $\mathcal{P}$  and  $\mathcal{M}$  enantiomers, the effects of the temperature in the energy barriers, and the thermal population. Conclusions are given in Section 4.

## II. THEORETICAL METHODS

### A. Global Minimum Search and Computational Details

All geometrical structures are optimized locally without imposing any symmetry, the self-consistent-field procedure was performed with a convergence criterion of  $10^{-6}$  a.u. The energy, maximum force and maximum displacement convergence were set to  $10^{-6}$  Ha, 0.002 Ha/Å and 0.0005 Å respectively. All calculations were performed using the Gaussian suite code<sup>48</sup> employing the Becke's hybrid three-parameter<sup>49,50</sup> exchange-correlation functional in combination with the Perdew and Wang GGA functional PW91,<sup>51,52</sup> this combination is known as B3PW91 exchange-correlation functional. The B3PW91 has been employed in other studies of reactivity in copper clusters with a good performance<sup>53,54</sup>, It is worth point out that hybrid functionals including a portion of Hartree-Fock exchange have shown a superior performance<sup>53,55,56</sup>. For the basis set, we employed the The LANL2DZ basis set is used for transition metals due to its low computational cost<sup>57</sup> With the aim to refine the optimization and the energies, we used Ahlrichs-type triple- $\zeta$  quality extended valence def2TZVP basis<sup>58,59</sup> that is more accurate for transition metals<sup>60</sup> despite it has a considerably higher computational cost.<sup>61</sup> In this study the dispersion corrections are taking into account through the D3 version of Grimme's dispersion<sup>62</sup> as it is implemented in Gaussian code. In a previous work, the effect of the dispersion corrections on the structural and energetic properties of the pure BeB clusters were studied founding that the energetic ordering of isomers can change when the dispersion is taking into account<sup>40,43</sup>. Transition states are discarded through a vibrational analysis, making sure that the minimum energy structure is a true structure minimum energy. Calculation of Gibbs free energy properties of  $\text{Cu}_{13}$  cluster requires an exhaustive and systematic sampling of the free en-

ergy surface with the aim to find all possible low-energy structures.<sup>43,63</sup> First of all, the search of the global minimum in atomic clusters is a complicated task due mainly that degrees of freedom of a molecule increases with the number of atoms; as a consequence, the number of local minimum increase exponentially with the number of atoms, moreover the calculated total energy of the cluster requires high level of quantum mechanical methodology to produce a real energy. In spite of that, several algorithms coupled with DFT to search the lowest energy structures on the potential energy surface of atomic clusters has been employed until nowadays, as kick methodology<sup>64-73</sup>, genetic algorithms<sup>43,74-77</sup>. Our computational procedure to elucidate the lowest energy consisted of employing a hybrid genetic algorithm called *GALGOSON*<sup>40,43</sup>. *GALGOSON* employ a multi-step search strategy where in the first step it makes optimizations employing LANL2DZ basis set and in second step-refine it employs the def2TZVP basis set, the creation of the initial population take into account the 2D and 3D structures<sup>72,74</sup> with an initial population of 650 random structures for the Cu<sub>13</sub> cluster and the criterion to stop the algorithm is until the five generations converged. This methodology based on previous works<sup>72,75,78,79</sup> consists of a multi-step approach (cascade) to efficiently sample the potential/free energy surface coupled to the *Gaussian* code<sup>48</sup>. Chemical bonding was examined using the Adaptive Natural Density Partitioning (AdNDP) method<sup>40,80</sup>. AdNDP analyses the first-order reduced density matrix and recovers Lewis bonding (1c-2e or 2c-2 e, i.e., lone pairs (LPs) or two-center two-electron bonds) and delocalized bonding elements (associated with the concept of electron delocalization).

In this study, the fundamental thermodynamic properties such as enthalpy H, and entropy S and Gibbs free energy dependent on temperature were computed within the framework of nanothermodynamics<sup>40,43,81-84</sup> through the partition function Q given in Equation 1, and described in refs.<sup>43,81,85</sup> or any standard text relating to thermodynamics<sup>86,87</sup>

$$Q(T) = \sum_i g_i e^{-\Delta E_i / K_B T} \quad (1)$$

In Eq. 1,  $g_i$  is the degeneracy factor,  $k_B$  is the Boltzmann constant,  $T$  is the temperature, and  $-\Delta E_i$  is the total energy of a cluster.<sup>43,82,86</sup> The total partition function Q is the product of the qtrasn, qrot, qvib, and qelec<sup>40,43,85</sup> computed under the rigid rotor, harmonic oscillator, Born-Oppenheimer, ideal gas, and particle-in-a-box approximations<sup>40,43</sup>. The thermal populations P(T) at absolute temperature T or the so called probability of a particular isomer is computed with Equation 2:

$$P(T) = \frac{e^{-\beta \Delta G^k}}{\sum e^{-\beta \Delta G^k}}, \quad (2)$$

where  $\beta = 1/k_B T$ , and  $k_B$  is the Boltzmann constant,

$T$  is the absolute temperature,  $\Delta G^k$  is the Gibbs free energy of the  $k^{th}$  isomer. Equation 2 establishes that the distribution of molecules among energy levels is a function of the energy and temperature<sup>40,43,88</sup>.

### III. RESULTS AND DISCUSSION

#### A. The lowest energy structures and energetics

The most important low-energy structures of a neutral Cu<sub>13</sub> cluster optimized at the B3PW91-GD3/def2TZVP level of theory found in this study are shown in Figure 1. At room temperature, the isomers depicted in Figure 1 contributed to 94% of the molecular properties in a Boltzmann ensemble; thus, almost all molecular properties were due to those isomers. Additionally, they are chiral structures. The putative chiral global minimum is depicted in Figure 1a with symmetry C<sub>1</sub>. These are bilayered structures composed of a shared pentagonal bipyramid interspersed with a distorted hexagonal ring with a Cu atom capping one of its faces and two Cu atoms capping the other face of the hexagonal ring, in good agreement with similar structures<sup>28,89,90</sup>. The pentagonal bipyramid interspersed with the hexagonal ring is built with 12 Cu atoms. One more Cu atom caps the pentagonal bipyramid; this capping Cu atom is responsible for the chirality of the Cu<sub>13</sub> cluster. Our calculated Cu-Cu bond length on the putative chiral global minimum is 2.432 Å, in good agreement with other reported DFT calculations of a Cu-Cu dimer of 2.248 Å<sup>91</sup> and also with an experimental bond length of 2.22 Å<sup>92,93</sup>, just slightly above 5.3% of the experimentally determined value. The calculated vibrational frequency of Cu<sub>13</sub> was 60 cm<sup>-1</sup>, whereas the computed vibrational frequency of the Cu-Cu dimer was 245 cm<sup>-1</sup>, again in good agreement with the experimental value of 265 cm<sup>-1</sup><sup>93</sup>. We also explored the higher multiplicity of quartets and found that the lowest energy structure lay 20.5 kcal/mol above the doublet putative chiral global minimum energy structure. The second structure that was higher in free energy lay at 0.41 kcal/mol at room temperature; it was also a bilayered structure, similar to the putative global minimum, but with C<sub>2</sub> symmetry. Iwasa et al.<sup>94</sup> reported a similar double-layer structure as a putative global minimum with C<sub>2</sub> symmetry, but without taking into account the temperature. One of our previous studies showed that these tiny Gibbs free energy differences are derived from rotational entropy<sup>40</sup>. The C<sub>1</sub> and C<sub>2</sub> symmetry clusters adopted a hollow layered structure. The following higher energy isomer lay at 1.0 kcal/mol at room temperature and was an achiral buckled-biplanar (BBP) structure with C<sub>s</sub> symmetry, which agrees with previous work<sup>95</sup>. At room temperature, its contributions to the molecular properties were less than 6%. The average bond length on isomer BBP was 2.432 Å, similar to the average bond length of the chiral putative global minimum. Next, higher energy structures lay 3.9

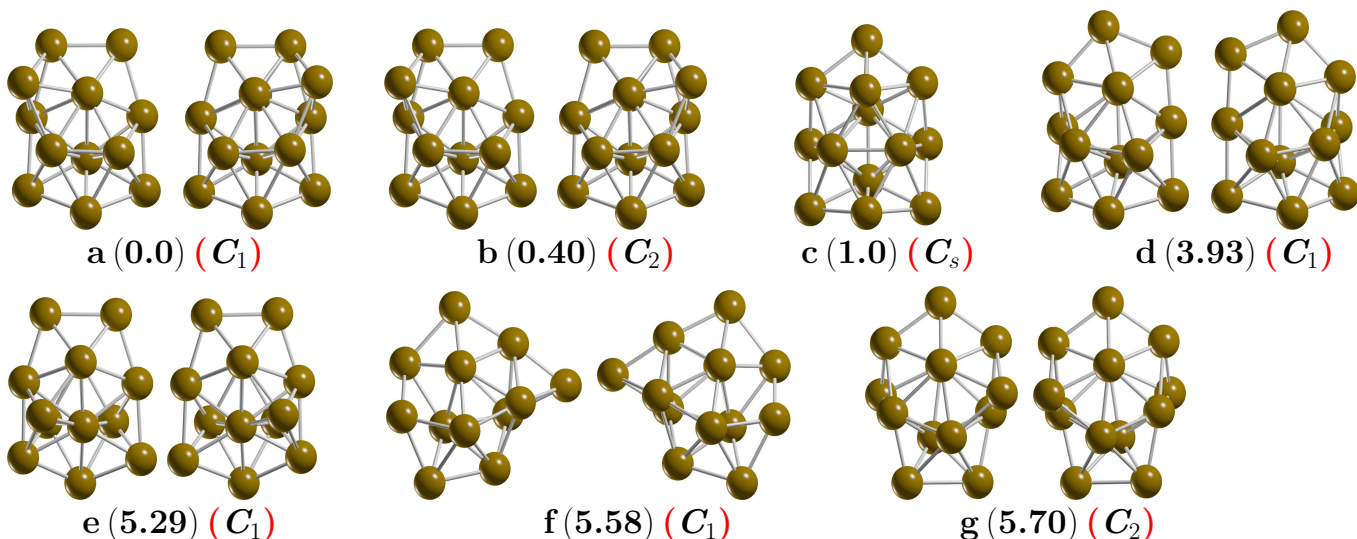


FIG. 1: (Color online) The chiral lowest energy structure is depicted in a), the chiral low-energy structures are depicted in b,d,e,f,g whereas the achiral structure is depicted in c). Those structures were optimized at the B3PW91-D3/def2TZVP level of theory. The first letter indicates the isomer, the relative Gibbs free energies in kcal/mol appear in round parentheses computed at 298.15 K, and the point group symmetry in red round parentheses. The isomers, represented in a) and b), differ only in molecular symmetry. The isomer with  $C_2$  symmetry has a Gibbs free energy equal to less than the non-symmetric  $C_1$  isomer. The RMSD between the isomer with symmetry  $C_1$  and the isomer with symmetry  $C_2$  is 0.0014. The atomic XYZ coordinates are given in Appendix B.

kcal/mol above the chiral putative global minimum, and their average bond length was 2.444 Å, slightly larger than the average bond length of 2.432 Å of the putative global minimum. This also appeared as a bilayered chiral structure with a shared hexagonal bipyramid interspersed with a hexagonal bipyramid. The following higher energy structure lay 5.29 kcal/mol above the putative minimum global. It was a bilayered structure consisting of 12 atoms, with 1 atom capping one of its faces. It is depicted in Figure 1e. Structures located at higher energy than 5.5 kcal/mol above the putative global minimum are depicted in Figure 1f,g. Those structures also adopted a layered structure with no interior atoms, with similar morphology to that of low-energy isomers. These two structures did not contribute to the molecular properties in the studied temperature range. The  $\text{Cu}_{13}$  cluster low-energy structures preferentially adopted morphologies of bilayered structures rather than highly symmetric 3D structures. In contrast,  $\text{Au}_{13}$  clusters prefer planar structures due to relativistic effects<sup>35</sup>; therefore, further studies are needed to investigate why bilayered structures in the  $\text{Cu}_{13}$  cluster are energetically preferred. For the  $\text{Cu}_{13}$  cluster, the icosahedron structure is not energetically favorable in the temperature range examined, which is consistent with previous work where the authors did not take into account the temperature<sup>1</sup>. In this study, the icosahedron structure was located at 24.6 kcal/mol above the putative global minimum at room temperature. To get an idea of the bonding situation in the chiral putative global minimum structure, we performed an

AdNDP analysis; the results are shown in Figure 2. This analysis revealed the presence of 5 sets of 13 1c-2e bonds with occupation numbers (ONs) between 1.98 and 1.99 —e—, i.e., lone pairs (LPs) corresponding to the fully filled 3d shell in each Cu atom. The bonding in this cluster was then due to the 4s shell electrons for which the bonding pattern, as revealed by AdNDP, consisted of 6 sets of 13c-2e completely delocalized bonds, plus a 9c-1e bond corresponding to the unpaired electron which, as shown in Figure 2, was mostly delocalized in the peripheral atoms of the cluster.

## B. Energetics

Temperature drastically affects the Gibbs free energy of the isomers; therefore, in a molecular ensemble (collection), the energetic ordering of isomers changes. Besides, from a theoretical point of view, the energetic ordering can also change when computing energies using different levels of theory<sup>43,96</sup>. To wit, energy computed at different methods yield different energies due mainly to the functional and basis-set employed,<sup>43</sup> so the energetic ordering change; consequently, the probability of occurrence and the molecular properties will change. Moreover, we compute the  $\mathcal{T}_1$  diagnostic to determine if the computed DFT energies are properly described by a single reference method or contain a multireference character.

To gain further insight into the energetic ordering of the low-lying isomers, we optimized the low-lying en-

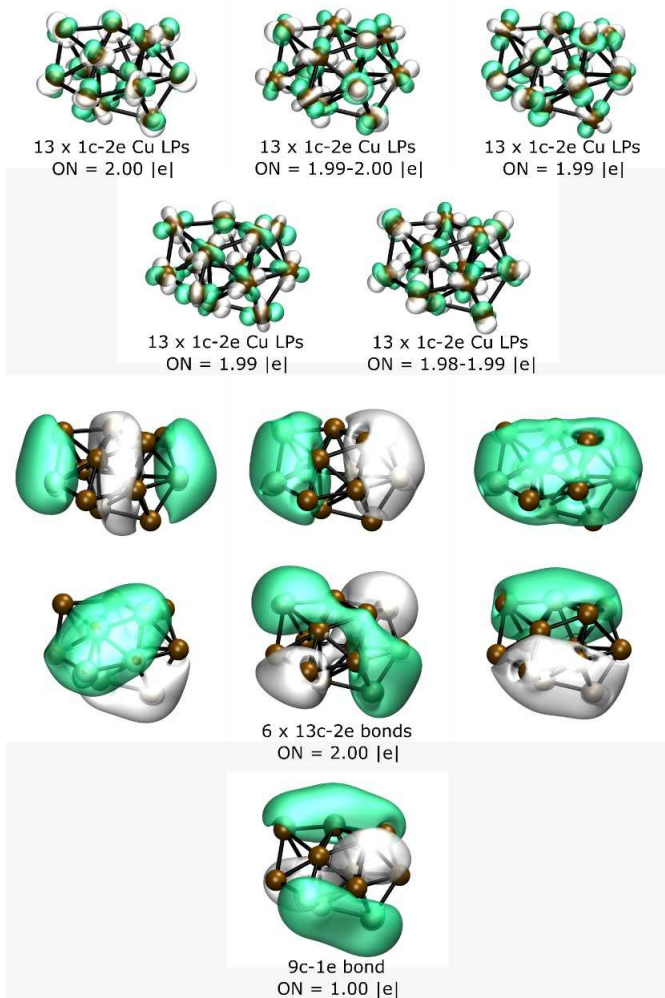


FIG. 2: (Color online) Results of the AdNDP analysis of the lowest-energy chiral isomer of the  $\text{Cu}_{13}$  system.

ergy structures employing three more DFT functionals: TPSS<sup>97</sup>, PBE<sup>98</sup>, and BP86<sup>50</sup> with def2-TZVP basis set, and single point (SP) relative energies computed employing the domain-based local pair natural orbital coupled-cluster theory (DLPNO-CCSD(T)), with TightPNO setting<sup>47</sup>, and with and without ZPE energy correction. The purpose was to ascertain the origin of the slight 0.41 kcal/mol differences (below the chemical accuracy of 1 kcal/mol) in the relative Gibbs free energy (Table I) and that these are not due to numerical errors, algorithmic approximations, integration grids, or functional and basis set dependence, to name a few. In Table I, lines first through the fourth show the relative Gibbs free energies computed at B3PW91-D3/def2-TZVP, TPSS-D3/def2-TZVP, PBE-D3/def2-TZVP, and BP86-D3/def2-TZVP, respectively. DLPNO-CCSD(T) relative energies, with and without ZPE correction, are shown in the fifth and sixth line of Table I, electronic with zero-point energy and electronic energy, at the B3PW91-D3/def2-TZVP level of

theory are shown in the seventh and eighth lines of Table I, and line ninth shows the point group symmetry, the  $\mathcal{T}_1$  diagnostic for each isomer is shown in line tenth of Table I, our results confirm that the computed  $\mathcal{T}_1$  diagnostic values are slightly above the recommended threshold of 0.02<sup>40,99</sup>; So, these values suggest that multireferential studies have to be carried out for  $\text{Cu}_{13}$  cluster. At the CCSD(T) theoretical level, the lowest-energy structure is the pair of enantiomers with symmetry  $C_2$ ; despite that, at finite temperature, the lowest energy structure is the pair of enantiomers with symmetry  $C_1$ . A more detailed analysis of the results in Table I shows that the relative electronic energy of the four chiral low-energy isomers labeled in Table I (a, b, c, d), with symmetry  $C_1$ ,  $C_1$ ,  $C_2$ , and  $C_2$ , respectively, is zero, considering the ZPE; also the relative electronic energy is zero. In contrast, the relative Gibbs free energy at 298.15 K shown in the fifth column is 0.41 kcal/mol. The relative Gibbs free energy at 298.15 K for the TPSS, PBE, BP86 DFT-functions, between the putative global minimum and the second isomer, is also 0.41 kcal/mol. This Gibbs free energy difference does not depend on the functional employed, as shown in Table I. At temperature  $T=0$ , the total energy of an isomer is the electronic energy plus ZPE ( $\epsilon_0 + ZPE$ ). If the temperature increases, entropic effects start to play, and Gibbs's free energy determines the global minimum. At any temperature  $T$ , the isomers, represented in Figure 1 and Figure 1b, differ only in molecular symmetry. The isomer with  $C_2$  symmetry has a Gibbs free energy equal to  $RT\ln(\sigma)$  less than the non-symmetric  $C_1$  isomer. Here  $R$  is the universal gas constant,  $T$  temperature, and  $\sigma$  is the symmetry number. The symmetry number appears in the denominator of the molecular rotational partition function<sup>40,43,100,101</sup>. This implies that the less symmetric isomers at finite temperature are more thermodynamically stable than the more symmetric ones due to the energy factor given by  $RT\ln(\sigma)$ . The factor becomes zero at  $T=0$  and increases linearly with temperature. Figure 3 shows the factor as a function of temperature and for different symmetry numbers. Moreover the  $\mathcal{T}_1$  diagnostic indicate that a multireference c For our optimized low-energy isomers with  $C_2$  symmetry, the symmetry number is 2, so the Gibbs free energy at 298.15 K with and without symmetry will differ by 0.41 kcal/mol regardless of the DFT method. This value is higher at high temperatures and with higher symmetry numbers. For example, the benzene molecule with  $D_{6h}$  symmetry has a symmetry number 12, the Gibbs free energy at 298.15 K with and without symmetry will differ by 1.47 kcal/mol, which is greater than the chemical precision. Here, we call this the effect of the symmetry number on the Gibbs free energy and on the thermal populations at finite temperature; the symmetry number appears when identical atoms are considered indistinguishable and are determined solely by the point group symmetry of the molecule. We emphasize the importance of symmetry in calculating thermal populations at absolute temperature  $T$  or the so called population probability

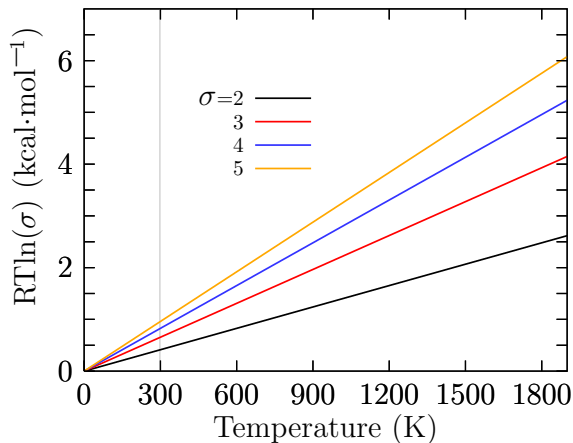


FIG. 3: (Color online) The difference of the Gibbs free energy computed with and without symmetries is given by a factor of  $RT\ln(\sigma)$ ; in this factor,  $R$  is the universal gas constant,  $T$ , the temperature, and  $\sigma$  is the symmetry number (The factor is similar to the enantioselectivity. These values, at 298.15 K, are in good agreement with the value 0.41 kcal/mol shown in the Table I.

or relative populations, hence the molecular properties. For example, the melting temperature for a symmetrical molecule is higher than a non-symmetrical molecule; moreover, the activation energy barrier could be higher when we consider a non-symmetrical molecule in the calculation of the transition state. The energy computed at different theoretical levels influences the energy distribution of the isomers and, as a consequence, the Boltzmann weights. For the four DFT functionals used in this study, the energy ordering is preserved, although differences in the energy between the isomers occur; for each DFT functional, the main contributors to any molecular property of  $\text{Cu}_{13}$  are always the chiral isomers depicted in Figure 1a.

### C. Structures and Stability at Finite Temperature.

In chemistry, physics, and biology, the lowest energy structure and all the low-energy structures near the global minimum are crucial because all molecular properties are statistical averages derived from the ensemble of molecular conformations<sup>40</sup>. The probability of occurrence of each particular isomer is depicted in Figure 4 for the  $\text{Cu}_{13}$  cluster. It was determined by employing Equation 2 and temperatures ranging from 20 to 1500 K at the B3PW91-D3/def2TZVP level of theory. Figure 4 shows the probability of occurrence considering all chiral and achiral structures. The analysis of these results led to an interesting observation. The pair of enantiomers that appeared as the putative global minimum at temperature 0 K was strongly dominant in the temperature range from 20 to 1500 K. Moreover, there were no solid-solid transformation points in any temperature range, which

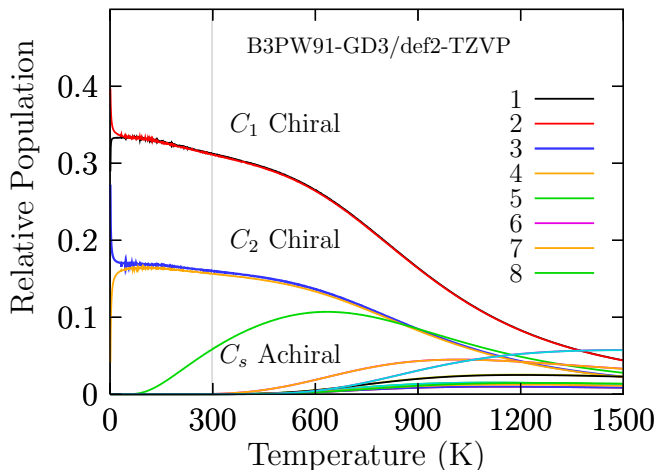


FIG. 4: (Color online) Probability of occurrence for all isomers at temperatures ranging from 20 to 1500 K. The red and black solid lines depict the probability occurrence of the putative chiral global minimum with symmetry  $C_1$  and strongly dominate in all ranges of temperatures. The bulk melting temperature of copper is 1358 K<sup>102</sup>; thus, our results below this temperature are consistent. Probability of occurrence with DFT functionals: TPSS, PBE, and BP86 are displayed in Figure 6.

means no interchange of dominant low-energy structures at high temperatures. A closer inspection of Figure 4 shows that the decay of probability of occurrence of the pair of enantiomers with symmetry  $C_1$ , depicted by a red solid line, is closer to linear rather than exponential for temperatures ranging from 20 to 600 K. Above 600 K and up to 1500 K, the decay is exponential. At 300 K, the chiral structure has a probability of 32%, whereas the second isomer located 0.4 kcal/mol above the putative global minimum has a probability of 16%. The above discussion shows that all molecular properties of the  $\text{Cu}_{13}$  cluster are attributed to the chiral putative global minimum at absolute temperature zero. The probability of occurrence of the chiral putative global structures, is depicted by blue and yellow solid lines in Figure 4. The probability of occurrence for structures with  $C_1$  and  $C_2$  symmetries showed similar behaviors but different values; even so, the molecular properties are attributed to only one pair of enantiomers with symmetry  $C_1$ . The probability of occurrence for the achiral structure, which is shown in Figure 1c, located 1 kcal/mol above the putative global minimum, is depicted by a green solid line in Figure 4; it started to increase around a temperature of 120 K, and at room temperature, it has a probability of 5%. At 700 K, the highest probability of occurrence was reached, corresponding to 12%; above this temperature, up to 1500 K, it started to decrease. Note that above 800 K and up to 1200 K, the achiral structure with  $C_s$  symmetry and the putative global minimum structures with  $C_2$  symmetries coexisted. Interestingly, the Boltzmann ensemble was composed of an equal mixture of  $\mathcal{M}$  and

TABLE I: Relative energy in kcal/mol of the low-lying isomers depicted in Figure 1 labeled from a to f, employing various density functionals: B3PW91, TPSS, PBE, and BP86, with the def2TZVP basis set. CCSD(T) employing the domain-based local pair natural orbital coupled-cluster theory (DLPNO-CCSD(T)), with TightPNO setting, with zero point energy (DLPNO-CCSD(T)+ $\mathcal{E}_{\text{ZPE}}$ ). Electronic energy with ZPE ( $\mathcal{E}_0 + \mathcal{E}_{\text{ZPE}}$ ), Electronic energy ( $\mathcal{E}_0$ ), point group symmetry, and  $\mathcal{T}_1$  Diagnostic.

Level	Isomers									
	$i_a$	$i_a$	$i_b$	$i_b$	$i_c$	$i_d$	$i_d$	$i_e$	$i_e$	$i_f$
$\Delta G(\text{B3PW91})$	0.0	0.0	0.3953	0.4091	0.9946	3.9338	3.9357	5.2967	5.2967	5.5728
$\Delta G(\text{TPSS})$	0.0	0.0	0.4010	0.4016	0.7248	5.6017	5.6029	5.5477	5.5477	7.5438
$\Delta G(\text{PBE})$	0.0	0.0	0.4145	0.4217	0.5491	3.8478	3.8491	5.5283	5.7284	5.7310
$\Delta G(\text{BP86})$	0.0	0.0	0.4079	0.4035	0.8634	3.5611	5.4291	5.4291	5.2817	7.2798
DLPNO-CCSD(T)	0.0	-0.1298	-0.2154	-0.2144	0.6827	5.0246	5.8771			
DLPNO-CCSD(T)+ $\mathcal{E}_{\text{ZPE}}$	0.0	-0.1298	-0.2216	-0.2170	0.7084	4.9022	5.7886			
$\mathcal{E}_0 + \mathcal{E}_{\text{ZPE}}$	0.0	0.0	0.0	0.0	0.9262	4.5877	4.5877	5.6124	5.6124	6.3327
$\mathcal{E}_0$	0.0	0.0	0.0	0.0	0.9002	4.7096	4.7098	5.7013	6.4969	6.4966
Point group symmetry	$C_1$	$C_1$	$C_2$	$C_2$	$C_s$	$C_1$	$C_1$	$C_1$	$C_1$	$C_1$
$\mathcal{T}_1$ Diagnostic	0.023	0.023	0.023	0.023	0.023	0.023	0.023	0.023	0.023	0.023

$\mathcal{P}$  enantiomers; thus, the chiral properties were null in all ranges of temperature, i.e., the  $\text{Cu}_{13}$  cluster did not exhibit properties such as vibrational/electronic circular dichroism. In ranging temperatures from 1200 to 1500 K, all isomers coexist with less than ten percent probability. To wit, all isomers are equally populated for hot temperatures or when the temperature increases to large values. The bulk melting temperature of copper, 1358 K<sup>102</sup>; So, we must consider that the anharmonic effects become strong at high temperatures<sup>40</sup>. From the thermal population, we consider the entropic-temperature term has a small effect on the  $\text{Cu}_{13}$  cluster distribution of isomers on the scale of temperature, as shown in Figure 4.

#### D. Enantiomerization Energy Barrier at Finite Temperature.

The process in which one enantiomer in a pair is converted into the other is known as enantiomerization; enantiomers each have an equal probability of occurrence, and the same energy. The enantiomerization energy or activation energy at temperature T defines the configurational stability. In some cases, a low enantiomerization energy is undesirable<sup>103</sup>. Two reaction mechanisms compete for the interconversion from  $\mathcal{P}$  to  $\mathcal{M}$  structures, and the shape of the energy barriers (or IRC) is similar to the inverted double-well potential<sup>104</sup> Figure 5a shows the reaction mechanism for the interconversion between  $\mathcal{P}$  and  $\mathcal{M}$  structures for route A, which proceeds via a two-step mechanism consisting of two symmetric steps with only one intermediate. Figure 5a shows the reaction mechanism for the interconversion between  $\mathcal{P}$  and  $\mathcal{M}$  structures for route B, which proceeds via a two-step mechanism consisting of two symmetric steps with only

one intermediate. Figure 5a depicts the transition states TS1 and TS2, the intermediate (Int), and the putative lowest energy pair of enantiomers  $\mathcal{P}$  and  $\mathcal{M}$ . The energy of enantiomerization was 12.15 kcal/mol, whereas the activation energy for the interconversion of the intermediate to  $\mathcal{P}/\mathcal{M}$  structures was 5 kcal/mol at room temperature. The intermediate state was located at 7.13 kcal/mol above the putative chiral lowest energy structure. The structures of the TS1 and TS2 states are depicted in Figure 5a. They appeared to be bilayer structures composed of a shared pentagonal bipyramid interspersed with a distorted hexagonal ring. The green atom represents the Cu atom that caps one edge of the pentagonal bipyramid and is responsible for the chirality of the  $\text{Cu}_{13}$  cluster. The intermediate state structure for the same bilayer presented 12 Cu atoms and the green Cu atom caps one of the faces in the pentagonal bipyramid. Figure 5a shows the enantiomerization energy  $E_{ae}$  depicted by a solid blue line. The relative energy of the intermediate,  $E_{Int}$ , for the putative global chiral structures is depicted by a solid red line. As the temperature increased, the enantiomerization energy increased almost linearly. In contrast, the relative energy of the intermediate with respect to the putative global minimum decreased linearly, implying that the inverted double-wall became energetically greater. The activation energy for the interconversion between the intermediate and the  $\mathcal{M}$  structure was 5 kcal/mol at room temperature; this increased linearly, from 4 kcal/mol at a temperature of 100 K to 9.5 kcal/mol at a temperature of 1200 K. As a consequence. In contrast, at low temperatures, the enantiomerization energy trend reached a minimum, whereas the relative energy of the intermediate increased; thus, the energy activation for the interconversion of the intermediate to the  $\mathcal{P}/\mathcal{M}$  states tended to be smaller. These results suggest that at high temper-

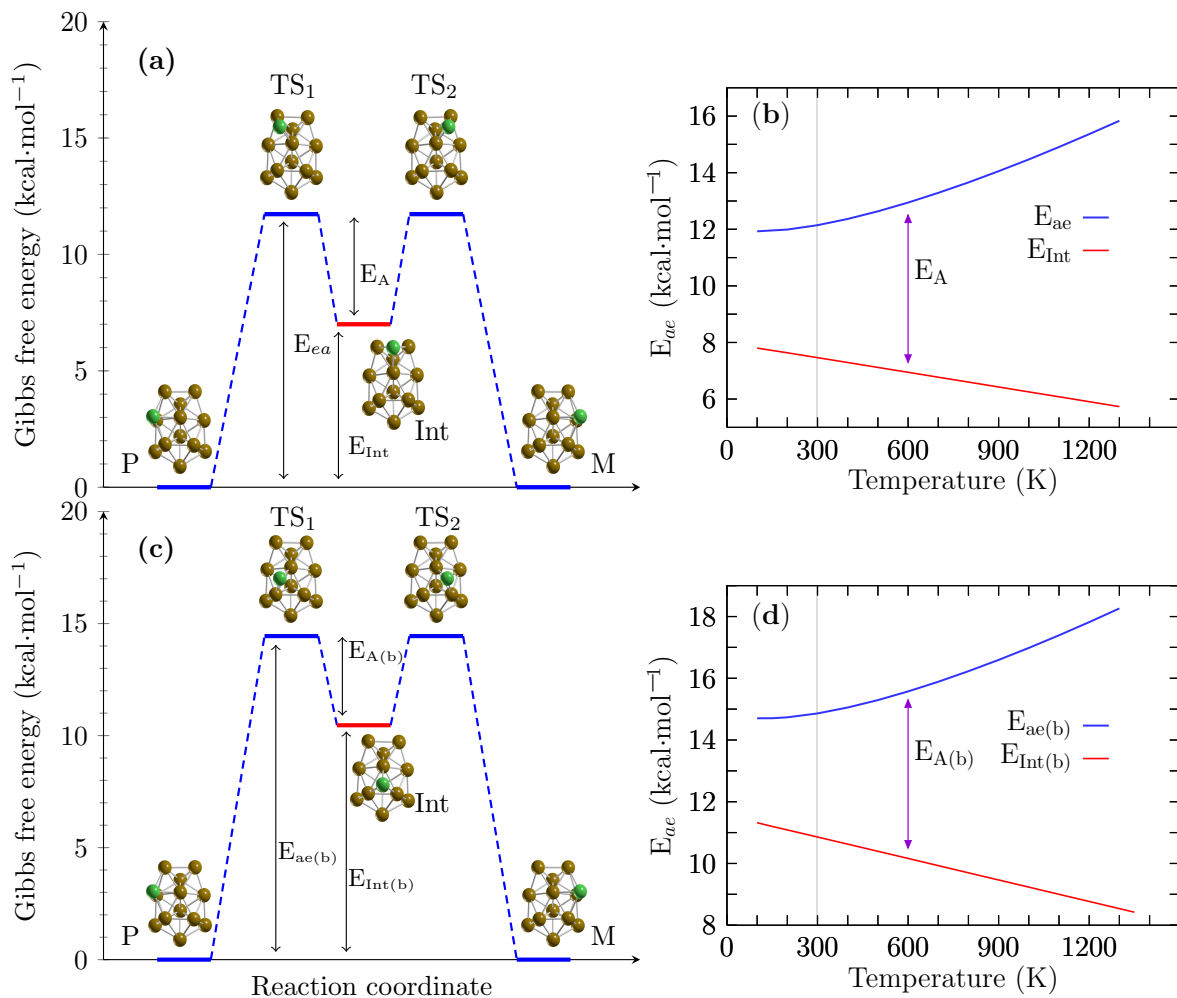


FIG. 5: (Color online)(Color online) Figure (a) shows the energy profile of a chemical reaction (route A) with two symmetric transition states ( $TS_1$ ,  $TS_2$ ) and one intermediate ( $Int$ ) for the interconversion between the lowest energy  $\mathcal{P}$  and  $\mathcal{M}$  enantiomers. Figure (c) shows the energy profile of a chemical reaction (route B) with two symmetric transition states ( $TS_1$ ,  $TS_2$ ) and one intermediate ( $Int$ ) for the interconversion between the lowest energy  $\mathcal{P}$  and  $\mathcal{M}$  enantiomers. In (b), the enantiomerization energy ( $E_{ea}$ ) is 12.14 kcal/mol at room temperature. In contrast, the intermediate structure lay at 7.13 kcal/mol ( $E_{Int}$ ) above the putative global minimum  $\mathcal{P}$  and  $\mathcal{M}$  structures, so the activation energy in the interconversion from the intermediate ( $Int$ ) to the  $\mathcal{P}$  or  $\mathcal{M}$  structure was 5.0 kcal/mol, at room temperature. Figure (b) displays the enantiomerization energy ( $E_{ea}$ , route A) depicted by a blue-solid line. The relative energy of the intermediate structure ( $E_{Int}$ ) with respect to the putative global minimum is depicted by a red solid line. Figure (d) displays the enantiomerization energy ( $E_{ea}$ , route B) depicted by a blue-solid line. The activation energy barrier ( $E_A$ ) between the intermediate structure and the  $\mathcal{P}$  or  $\mathcal{M}$  structure is indicated by the violet arrow and is the difference between  $E_{ea}$  and  $E_{Int}$  for temperatures ranging from 100 to 1300 K. The green and copper-colored spheres represent the copper atoms. Green represents a Cu atom that is moving; the chirality is due to this atom.

atures, the enantiomerization barrier energy increased, and the intermediate state energy became more significant, stabilizing chirality and allowing the separation of enantiomers at room temperature. To elucidate the behavior of the interconversion from  $\mathcal{P}$  and  $\mathcal{M}$  structures; We computed the reaction rate constants based on Equation 3 (Eyring equation) that used the activation barrier  $\Delta G$  between the putative global minimum  $\mathcal{P}/\mathcal{M}$  structures and the transition state and did not take into account the tunneling effect. The Eyring equation relates

the rate constant to temperature and the activation free energy.

$$k = k_0 \frac{K_B T}{h} e^{-\Delta G/RT} \quad (3)$$

In Equation 3,  $k$  is the rate constant,  $k_0$  transmission coefficient that in the absence of other kinetic data is set to 1,  $K_B$  is Boltzmann constant,  $T$  is the temperature,  $h$  is the Planck constant,  $R$  is ideal gas constant, and  $\Delta G$  is the activation energy barrier. We consider

Level of theory	Reaction A			Reaction B		
	$E_{ea}$	$E_{Int}$	$E_A$	$E_{ea}$	$E_{Int}$	$E_A$
B3PW91-D3/Def2TZVP	12.15	7.13	5.0	14.85	10.86	3.99
B3PW91/Def2TZVP	12.36	6.38	5.97	15.60	11.31	4.28

TABLE II: Table shows the values of enantiomerization energy ( $E_{ea}$ ), relative energy of intermediate ( $E_{Int}$ ), and activation energy ( $E_A$ ), for two mechanism of reaction A and B, and with and without taking into account the D3 Grimme’s dispersion. The inclusion of dispersion lower the energy barriers, i.e in B the  $E_A$  decreases 7%. (from 4.28 to 3.99 kcal/mol)

the rate-determining step in the overall reaction is the rate of interconversion between  $\mathcal{P}/\mathcal{M}$  and intermediary structures, and it is the slowest step; besides, its high activation energy characterizes it. (Notice, the activation energy barrier  $\Delta G$  is computed with the statistical thermodynamics). The height of the activation energy barrier at room temperature for interconversion between  $\mathcal{P}/\mathcal{M}$  and intermediary structures in route A is 12.14 kcal/mol, which leads to a rate constant of  $7.84 \times 10^3$  1/s, whereas the activation energy barrier at 900 K is 14.0 kcal/mol, which leads to a rate constant of  $7.47 \times 10^9$  1/s. This show that the rate constant increases at high temperatures, and it agrees with the thermal populations where the contribution of all isomers is less than 10% at high temperatures. We also have to consider that the melting point for copper is 1358 K, thus around this temperature, the glass state will dominate. Regarding dispersion, if it is not considered, the energy barriers tend to increase. For ease of comparison, Table 2 shows the values of the two similar reaction mechanisms A and B, taking into account the D3 dispersion of Grimme. Energetically, the reaction mechanism of route B is not so different from that of route A, as we can see in Figure 5c,d and in Table II.

#### IV. CONCLUSIONS

For the first time, to our knowledge and from our results, we computed the effect of symmetry on the Boltzmann populations on TM Cu clusters. Our computed  $\mathcal{T}_1$  diagnostic 0.023, determine that the computed DFT energies are not properly described by a single reference method or contain a multireference character. So, further studies needed to be done. We explored the potential and free energy surface of the neutral  $\text{Cu}_{13}$  cluster with an efficient cascade-type algorithm coupled to DFT. We found that the putative global minimum was a pair of enantiomers that strongly dominated at room temperature. Our findings show that the chirality exhibited by the  $\text{Cu}_{13}$  cluster emerged from the Cu atom capping a face of the core  $\text{Cu}_{12}$  cluster. We showed that for the interconversion between  $\mathcal{P}$  and  $\mathcal{M}$  structures, two similar reaction mechanisms were possible. Both of them closed in their energy barriers and proceeded via two symmetric steps. The energy of enantiomerization and the energy

barrier between the intermediate and the  $\mathcal{P}/\mathcal{M}$  structures increased as the temperature increased. We computed the reaction rate constants based on the Eyring equation; our findings show that at high temperatures, enantiomerization is favored. The entropic-temperature term did not significantly influence the energy barriers; thus, they are mainly composed of enthalpic energy. Regarding Grimme’s dispersion D3, this lowers the energy barriers, i.g., in route B, the  $E_A$  decreased by 7% (from 4.3 to 4.0 kcal/mol). We showed that the pair of enantiomers with  $C_1$  symmetries strongly dominated at room temperature revealed by the thermal population. Hence, at body temperature, all the molecular properties were attributable to those structures. For each DFT functional (B3PW91, TPSS, PBE, and BP86) used in this study, the thermal population and energetic ordering of the isomers are preserved, although differences in the energy between the isomers occur; the main contributors to any molecular property of  $\text{Cu}_{13}$  are always the chiral isomers. The bonding in the lowest energy chiral  $\text{Cu}_{13}$  cluster is due to the 4s shell electrons for which the bonding pattern, as revealed by AdNDP, consisted of 6 sets of 13c-2e completely delocalized bonds, plus a 9c-1e bond corresponding to the unpaired electron. Future work will focus on the computation of UV absorption of the Cu clusters employing Boltzmann weighted spectra, comparing it with a single UV spectrum of the putative global minimum.

#### V. ACKNOWLEDGMENTS

C. E. B.-G. thanks Conacyt for the Ph.D. scholarship (860052). E. P.-S. thanks Conacyt for the Ph.D. scholarship (1008864). E. R.-CH. thanks Conacyt for the Ph.D. scholarship (1075701). We are grateful to Dra. Carmen Heras, and L.C.C. Daniel Mendoza for granting us access to their clusters and computational support. Computational resources for this work were provided by *ACARUS* through the High-Performance Computing Area of the University of Sonora, Sonora, México. We are also grateful to the computational chemistry laboratory for providing computational resources, *ELBAKYAN*, and *PAKAL* supercomputers. Powered@NLHPC: This research was partially supported by the supercomputing infrastructure of the NLHPC (ECM-02) in Chile.

## VI. CONFLICTS OF INTEREST

The authors declare no conflict of interest.

## VII. FUNDING

This research received no external funding.

## VIII. SUPPLEMENTARY MATERIALS

The following are available online [for route A](#), and [for route B](#). All xyz atomic coordinates optimized of the

Cu<sub>13</sub>B<sub>8</sub> cluster at the B3PW91-D3/def2-TZVP/Freq.

## IX. ABBREVIATIONS

The following abbreviations are used in this manuscript:

Density Functional Theory (DFT), Domain-based Local Pair Natural Orbital Coupled-Cluster Theory (DLPNO-CCSD(T)), Zero-Point Energy (ZPE), Global Genetic Algorithm of University of Sonora (GALGOSON), Adaptive Natural Density Partitioning (AdNDP).

---

\* email: [sollebac@gmail.com](mailto:sollebac@gmail.com), [josecabellos@uson.mx](mailto:josecabellos@uson.mx)

- <sup>1</sup> Anderson S. Chaves, Maurício J. Piotrowski, and Juarez L. F. Da Silva. Evolution of the structural, energetic, and electronic properties of the 3d, 4d, and 5d transition-metal clusters (30 TM<sub>n</sub> systems for n = 2-15): a density functional theory investigation. *Phys. Chem. Chem. Phys.*, 19:15484–15502, 2017.
- <sup>2</sup> Wei Chen and Shaowei Chen. Oxygen electroreduction catalyzed by gold nanoclusters: Strong core size effects. *Angewandte Chemie International Edition*, 48(24):4386–4389, 2009.
- <sup>3</sup> Claude R. Henry. Surface studies of supported model catalysts. *Surface Science Reports*, 31(7):231–325, 1998.
- <sup>4</sup> Beatriz Santiago González, María J. Rodríguez, Carmen Blanco, José Rivas, M. Arturo López-Quintela, and José M. Gaspar Martinho. One step synthesis of the smallest photoluminescent and paramagnetic pvp-protected gold atomic clusters. *Nano Letters*, 10(10):4217–4221, 2010. PMID: 20836542.
- <sup>5</sup> William L. Barnes, Alain Dereux, and Thomas W. Ebbesen. Surface plasmon subwavelength optics. *Nature*, 424(6950):824–830, Aug 2003.
- <sup>6</sup> Nicole Cathcart and Vladimir Kitaev. Silver nanoclusters: Single-stage scaleable synthesis of monodisperse species and their chiroptical properties. *The Journal of Physical Chemistry C*, 114(38):16010–16017, 2010.
- <sup>7</sup> Xun-Lei Ding, Wei Xue, Yan-Ping Ma, Zhe-Chen Wang, and Sheng-Gui He. Density functional study on cage and noncage (Fe<sub>42</sub>O<sub>3</sub>)<sub>n</sub> clusters. *The Journal of Chemical Physics*, 130(1):014303, 2009.
- <sup>8</sup> Abdul Majid, Sunbul Zahid, Salah Ud-Din Khan, and Shahab Ud-Din Khan. Theoretical study of (TM)FeO<sub>3</sub> (tm = 3d transition metals) molecular clusters. *Journal of Nanoparticle Research*, 22(6):145, May 2020.
- <sup>9</sup> Jiatao Zhang, Junfeng Liu, Qing Peng, Xun Wang, and Yadong Li. Nearly monodisperse Cu<sub>2</sub>O and CuO nanospheres: preparation and applications for sensitive gas sensors. *Chemistry of Materials*, 18(4):867–871, Feb 2006.
- <sup>10</sup> Manoj B. Gawande, Anandarup Goswami, François-Xavier Felpin, Tewodros Asefa, Xiaoxi Huang, Rafael Silva, Xiaoxin Zou, Radek Zboril, and Rajender S. Varma. Cu and Cu-based nanoparticles: Synthesis and applications in catalysis. *Chemical Reviews*, 116(6):3722–3811, 2016. PMID: 26935812.
- <sup>11</sup> Yizhong Lu and Wei Chen. Sub-nanometre sized metal clusters: from synthetic challenges to the unique property discoveries. *Chem. Soc. Rev.*, 41:3594–3623, 2012.
- <sup>12</sup> Zhenguang Wang, Bingkun Chen, and Andrey L. Rogach. Synthesis, optical properties and applications of light-emitting copper nanoclusters. *Nanoscale Horiz.*, 2:135–146, 2017.
- <sup>13</sup> Yu-Syuan Lin, Yu-Feng Lin, Amit Nain, Yu-Fen Huang, and Huan-Tsung Chang. A critical review of copper nanoclusters for monitoring of water quality. *Sensors and Actuators Reports*, 3:100026, 2021.
- <sup>14</sup> Masahiro Itoh, Vijay Kumar, Tadafumi Adschiri, and Yoshiyuki Kawazoe. Comprehensive study of sodium, copper, and silver clusters over a wide range of sizes 2<n<75. *The Journal of Chemical Physics*, 131(17):174510, 2009.
- <sup>15</sup> Karl Jug, Bernd Zimmermann, Patrizia Calaminici, and Andreas M. Köster. Structure and stability of small copper clusters. *The Journal of Chemical Physics*, 116(11):4497–4507, 2002.
- <sup>16</sup> Patrizia Calaminici, Florian Janetzko, Andreas M. Koster, Roberto Mejia-Olvera, and Bernardo Zuniga-Gutierrez. Density functional theory optimized basis sets for gradient corrected functionals: 3d transition metal systems. *The Journal of Chemical Physics*, 126(4):044108, 2007.
- <sup>17</sup> Carlo Massobrio, Alfredo Pasquarello, and Andrea Dal Corso. Structural and electronic properties of small cu<sub>n</sub> clusters using generalized-gradient approximations within density functional theory. *The Journal of Chemical Physics*, 109(16):6626–6630, 1998.
- <sup>18</sup> P. Calaminici, A. M. Koster, N. Russo, and D. R. Salahub. A density functional study of small copper clusters: Cu<sub>n</sub> (n<5). *The Journal of Chemical Physics*, 105(21):9546–9556, 1996.
- <sup>19</sup> Albert Poater, Miquel Duran, Pablo Jaque, Alejandro Toro-Labbé, and Miquel Sola. Molecular structure and bonding of copper cluster monocarbonyls Cu<sub>n</sub>CO (n = 1-9). *The Journal of Physical Chemistry B*, 110(13):6526–6536, 2006. PMID: 16570950.
- <sup>20</sup> Patrizia Calaminici, Andreas M. Koster, and Zeferino Gómez-Sandoval. Density functional study of the structure and properties of Cu<sub>9</sub> and Cu<sub>9</sub><sup>-</sup>. *Journal of Chemi-*

- cal Theory and Computation*, 3(3):905–913, 2007. PMID: 26627410.
- 21 M. Yang, F. Yang, K. A. Jackson, and J. Jellinek. Probing the structural evolution of  $\text{Cu}_N$ ,  $n=9-20$ , through a comparison of computed electron removal energies and experimental photoelectron spectra. *The Journal of Chemical Physics*, 132(6):064306, 2010.
  - 22 S. Lecoultre, A. Rydlo, C. Félix, J. Buttet, S. Gilb, and W. Harbich. Optical absorption of small copper clusters in neon:  $\text{Cu}_n$ , ( $n = 1-9$ ). *The Journal of Chemical Physics*, 134(7):074303, 2011.
  - 23 C. Binns. Nanoclusters deposited on surfaces. *Surface Science Reports*, 44(1):1–49, 2001.
  - 24 Matthias Brack. The physics of simple metal clusters: self-consistent jellium model and semiclassical approaches. *Rev. Mod. Phys.*, 65:677–732, Jul 1993.
  - 25 T.P. Martin. Shells of atoms. *Physics Reports*, 273(4):199–241, 1996.
  - 26 Masaki Sakurai, Koji Watanabe, Kenji Sumiyama, and Kenji Suzuki. Magic numbers in transition metal (Fe, Ti, Zr, Nb, and Ta) clusters observed by time-of-flight mass spectrometry. *The Journal of Chemical Physics*, 111(1):235–238, 1999.
  - 27 Sarah Darby, Thomas V. Mortimer-Jones, Roy L. Johnston, and Christopher Roberts. Theoretical study of Cu-Au nanoalloy clusters using a genetic algorithm. *The Journal of Chemical Physics*, 116(4):1536–1550, 2002.
  - 28 Galip H. Guvelioglu, Pingping Ma, Xiaoyi He, Robert C. Forrey, and Hansong Cheng. Evolution of small copper clusters and dissociative chemisorption of hydrogen. *Phys. Rev. Lett.*, 94:026103, Jan 2005.
  - 29 Masahiro Itoh, Vijay Kumar, and Yoshiyuki Kawazoe. Growth behaviors and electronic structures of Na and Cu nanoclusters: The role of sp-d hybridization. *International Journal of Modern Physics B*, 19(15n17):2421–2426, 2005.
  - 30 Mingli Yang, Koblar A. Jackson, Christof Koehler, Thomas Frauenheim, and Julius Jellinek. Structure and shape variations in intermediate-size copper clusters. *The Journal of Chemical Physics*, 124(2):024308, 2006.
  - 31 Minglong Jiang, Qun Zeng, Tingting Zhang, Mingli Yang, and Koblar Alan Jackson. Icosahedral to double-icosahedral shape transition of copper clusters. *The Journal of Chemical Physics*, 136(10):104501, 2012.
  - 32 Riguang Zhang, Mao Peng, Tian Duan, and Baojun Wang. Insight into size dependence of  $\text{C}_2$  oxygenate synthesis from syngas on cu cluster: The effect of cluster size on the selectivity. *Applied Surface Science*, 407:282–296, 2017.
  - 33 Chen Shuangjing, Chen Xin, and Zhang Hui. Probing the activity of  $\text{Ni}_{13}$ ,  $\text{Cu}_{13}$ , and  $\text{Ni}_{12}\text{Cu}$  clusters towards the ammonia decomposition reaction by density functional theory. *Journal of Materials Science*, 52(6):3162–3168, 2017.
  - 34 Keisuke Takahashi. First-principles design of  $\text{cu}_{12}\text{shell}\text{fecore}$  core-shell clusters assembled with  $\text{K}_3\text{O}$  into hexameric rings: Implications for gas-storage materials. *ACS Applied Nano Materials*, 3(1):55–58, 2020.
  - 35 J P Chou, C R Hsing, C M Wei, C Cheng, and C M Chang. Ab initio random structure search for 13-atom clusters of FCC elements. *Journal of Physics: Condensed Matter*, 25(12):125305, feb 2013.
  - 36 J. Akola, H. Häkkinen, and M. Manninen. Ionization potential of aluminum clusters. *Phys. Rev. B*, 58:3601–3604, Aug 1998.
  - 37 Daniel Ebeling, Marina Šekutor, Marvin Stieffermann, Jalmar Tschakert, Jeremy E. P. Dah, Robert M. K. Carlson, André Schirmeisen, and Peter R. Schreiner. Assigning the absolute configuration of single aliphatic molecules by visual inspection. *Nature Communications*, 9(1):2420, Jun 2018.
  - 38 Wei-Li Li, Ya-Fan Zhao, Han-Shi Hu, Jun Li, and Lai-Sheng Wang.  $[\text{B}_{30}^-]$ : A quasiplanar chiral boron cluster. *Angewandte Chemie International Edition*, 53(22):5540–5545, 2014.
  - 39 Jorge Barroso, Jose Luis Cabellos, Sudip Pan, Fernando Murillo, Ximena Zarate, Maria A. Fernandez-Herrera, and Gabriel Merino. Revisiting the racemization mechanism of helicenes. *Chem. Commun.*, 54:188–191, 2018.
  - 40 Carlos Emiliano Buelna-Garcia, Eduardo Robles-Chaparro, Tristan Parra-Arellano, Jesus Manuel Quiroz-Castillo, Teresa del Castillo-Castro, Gerardo Martínez-Guajardo, Cesar Castillo-Quevedo, Aned de León-Flores, Gilberto Anzueto-Sánchez, Martha Fabiola Martin-del Campo-Solis, Ana Maria Mendoza-Wilson, Alejandro Vásquez-Espinal, and Jose Luis Cabellos. Theoretical prediction of structures, vibrational circular dichroism, and infrared spectra of chiral  $\text{Be}_4\text{B}_8$  cluster at different temperatures. *Molecules*, 26(13), 2021.
  - 41 Peng Lv, Zhansheng Lu, Feng Yang, Yi Zhang, Xinwei Yang, Guoliang Xu, and Zongxian Yang. A theoretical study of the lowest-energy PtPd co-doped silicon clusters: Chirality and fluxional transformation. *Physics Letters A*, 381(9):873–878, 2017.
  - 42 Yu-Jin Kong, Zhi-Ping Yan, Si Li, Hui-Fang Su, Kai Li, You-Xuan Zheng, and Shuang-Quan Zang. Photoresponsive propeller-like chiral AIE copper(I) clusters. *Angewandte Chemie International Edition*, 59(13):5336–5340, 2020.
  - 43 Carlos Emiliano Buelna-Garcia, Jose Luis Cabellos, Jesus Manuel Quiroz-Castillo, Gerardo Martinez-Guajardo, Cesar Castillo-Quevedo, Aned de Leon-Flores, Gilberto Anzueto-Sanchez, and Martha Fabiola Martin-del Campo-Solis. Exploration of free energy surface and thermal effects on relative population and infrared spectrum of the  $\text{Be}_6\text{B}_{11}^-$  fluxional cluster. *Materials*, 14(1), 2021.
  - 44 Francesca Baletto and Riccardo Ferrando. Structural properties of nanoclusters: Energetic, thermodynamic, and kinetic effects. *Rev. Mod. Phys.*, 77:371–423, May 2005.
  - 45 Yi Rao, Yimin Lei, Xiangyuan Cui, Zongwen Liu, and Fuyi Chen. Optical and magnetic properties of Cu-doped 13-atom Ag nanoclusters. *Journal of Alloys and Compounds*, 565:50–55, 2013.
  - 46 Wenlong Yang, Giovanna Longhi, Sergio Abbate, Andrea Lucotti, Matteo Tommasini, Claudio Villani, Vincent J. Catalano, Aleksandr O. Lykhin, Sergey A. Varganov, and Wesley A. Chalifoux. Chiral peropyrene: Synthesis, structure, and properties. *Journal of the American Chemical Society*, 139(37):13102–13109, 2017. PMID: 28829125.
  - 47 Dimitrios G. Liakos, Yang Guo, and Frank Neese. Comprehensive benchmark results for the domain based local pair natural orbital coupled cluster method (dlpno-ccsd(t)) for closed- and open-shell systems. *The Journal of Physical Chemistry A*, 124(1):90–100, 2020. PMID: 31841627.
  - 48 M. J. Frisch, G. W. Trucks, H. B. Schlegel, and

- G. E. Scuseria et al. Gaussian 09. *Gaussian Inc. Wallingford CT 2009*, jan 2009.
- <sup>49</sup> Axel D. Becke. Density-functional thermochemistry. iii. the role of exact exchange. *The Journal of Chemical Physics*, 98(7):5648–5652, 1993.
- <sup>50</sup> A. D. Becke. Density-functional exchange-energy approximation with correct asymptotic behavior. *Phys. Rev. A*, 38:3098–3100, Sep 1988.
- <sup>51</sup> John P. Perdew and Yue Wang. Accurate and simple analytic representation of the electron-gas correlation energy. *Phys. Rev. B*, 45:13244–13249, Jun 1992.
- <sup>52</sup> John P. Perdew, J. A. Chevary, S. H. Vosko, Kobljar A. Jackson, Mark R. Pederson, D. J. Singh, and Carlos Fiolhais. Atoms, molecules, solids, and surfaces: Applications of the generalized gradient approximation for exchange and correlation. *Phys. Rev. B*, 46:6671–6687, Sep 1992.
- <sup>53</sup> Estefanía Fernández, Mercedes Boronat, and Avelino Corma. Trends in the reactivity of molecular O<sub>2</sub> with copper clusters: Influence of size and shape. *The Journal of Physical Chemistry C*, 119(34):19832–19846, 2015.
- <sup>54</sup> Pablo Jaque and Alejandro Toro-Labbé. Characterization of copper clusters through the use of density functional theory reactivity descriptors. *The Journal of Chemical Physics*, 117(7):3208–3218, 2002.
- <sup>55</sup> Christopher J. Cramer and Donald G. Truhlar. Density functional theory for transition metals and transition metal chemistry. *Phys. Chem. Chem. Phys.*, 11:10757–10816, 2009.
- <sup>56</sup> Aron J. Cohen, Paula Mori-Sánchez, and Weitao Yang. Challenges for density functional theory. *Chemical Reviews*, 112(1):289–320, 2012. PMID: 22191548.
- <sup>57</sup> P. Jeffrey Hay and Willard R. Wadt. Ab initio effective core potentials for molecular calculations. potentials for the transition metal atoms sc to hg. *The Journal of Chemical Physics*, 82(1):270–283, 1985.
- <sup>58</sup> Florian Weigend and Reinhart Ahlrichs. Balanced basis sets of split valence, triple zeta valence and quadruple zeta valence quality for H to Rn: Design and assessment of accuracy. *Phys. Chem. Chem. Phys.*, 7:3297–3305, 2005.
- <sup>59</sup> Q. Zeng, X. Wang, M. L. Yang, and H. B. Fu. Interplay between geometrical and electronic stability of neutral and anionic Cu<sub>13</sub> clusters: a first-principles study. *The European Physical Journal D*, 58(1):125–129, May 2010.
- <sup>60</sup> Tayyibe Bardakc, Mustafa Kumru, and Ahmet Altun. Molecular structures, charge distributions, and vibrational analyses of the tetracoordinate Cu(II), Zn(II), Cd(II), and Hg(II) bromide complexes of p-toluidine investigated by density functional theory in comparison with experiments. *Journal of Molecular Structure*, 1116:292–302, 2016.
- <sup>61</sup> Piotr Matczak. Assessment of B3LYP combined with various ECP basis sets for systems containing Pd, Sn, and Pb. *Computational and Theoretical Chemistry*, 983:25–30, 2012.
- <sup>62</sup> Stefan Grimme, Jens Antony, Stephan Ehrlich, and Helge Krieg. A consistent and accurate ab initio parametrization of density functional dispersion correction (dft-d) for the 94 elements h-pu. *The Journal of Chemical Physics*, 132(15):154104, 2010.
- <sup>63</sup> Sven Heiles and Roy L. Johnston. Global optimization of clusters using electronic structure methods. *International Journal of Quantum Chemistry*, 113(18):2091–2109, 2013.
- <sup>64</sup> Alba Vargas-Caamal, Jose Luis Cabellos, Filiberto Ortiz-Chi, Henry S. Rzepa, Albeiro Restrepo, and Gabriel Merino. How many water molecules does it take to dissociate HCl? *Chemistry – A European Journal*, 22(8):2812–2818, 2016.
- <sup>65</sup> Estefanía Ravell, Said Jalife, Jorge Barroso, Mesías Orozco-Ic, Gerardo Hernández-Juárez, Filiberto Ortiz-Chi, Sudip Pan, Jose Luis Cabellos, and Gabriel Merino. Structure and bonding in CE<sub>5</sub>- (E=Al-Tl) clusters: Planar tetracoordinate carbon versus pentacoordinate carbon. *Chemistry - An Asian Journal*, 13(11):1467–1473, 2018.
- <sup>66</sup> Sudip Pan, Diego Moreno, Jose Luis Cabellos, Jonathan Romero, Andres Reyes, Gabriel Merino, and Pratim K. Chattaraj. In quest of strong Be-Ng bonds among the neutral Ng-Be complexes. *The Journal of Physical Chemistry A*, 118(2):487–494, 2014. PMID: 24199587.
- <sup>67</sup> Zhong-hua Cui, Yi-hong Ding, Jose Luis Cabellos, Edison Osorio, Rafael Islas, Albeiro Restrepo, and Gabriel Merino. Planar tetracoordinate carbons with a double bond in CA<sub>13</sub>E clusters. *Phys. Chem. Chem. Phys.*, 17:8769–8775, 2015.
- <sup>68</sup> Alba Vargas-Caamal, Filiberto Ortiz-Chi, Diego Moreno, Albeiro Restrepo, Gabriel Merino, and Jose Luis Cabellos. The rich and complex potential energy surface of the ethanol dimer. *Theoretical Chemistry Accounts*, 134(2):16, Jan 2015.
- <sup>69</sup> Zhong-hua Cui, Valentin Vassilev-Galindo, José Luis Cabellos, Edison Osorio, Mesías Orozco, Sudip Pan, Yi-hong Ding, and Gabriel Merino. Planar pentacoordinate carbon atoms embedded in a metallocene framework. *Chem. Commun.*, 53:138–141, 2017.
- <sup>70</sup> Alba Vargas-Caamal, Sudip Pan, Filiberto Ortiz-Chi, Jose Luis Cabellos, Roberto A. Boto, Julia Contreras-Garcia, Albeiro Restrepo, Pratim K. Chattaraj, and Gabriel Merino. How strong are the metallocene–metallocene interactions? cases of ferrocene, ruthenocene, and osmocene. *Phys. Chem. Chem. Phys.*, 18:550–556, 2016.
- <sup>71</sup> Elizabeth Florez, Nancy Acelas, Cesar Ibarguen, Sukanta Mondal, Jose Luis Cabellos, Gabriel Merino, and Albeiro Restrepo. Microsolvation of no<sub>3</sub>−: structural exploration and bonding analysis. *RSC Adv.*, 6:71913–71923, 2016.
- <sup>72</sup> Rafael Grande-Aztatzi, Paulina R. Martinez-Alanis, Jose Luis Cabellos, Edison Osorio, Ana Martínez, and Gabriel Merino. Structural evolution of small gold clusters doped by one and two boron atoms. *Journal of Computational Chemistry*, 35(32):2288–2296, 2014.
- <sup>73</sup> Rosa Elena Navarro, Octavio Serna-Medina, Yedith Soberanes, José Luis Cabellos, Motomichi Inoue, Hisila Santacruz, and Álvaro Posada-Amarillas. <sup>1</sup>H NMR of paramagnetic Dy<sup>3+</sup> complex with DTPA-amide p-xylylene-cyclophane; possible probing action toward d-histidine and histamine. *Polyhedron*, 181:114474, 2020.
- <sup>74</sup> Xue Dong, Said Jalife, Alejandro Vásquez-Espinal, Estefanía Ravell, Sudip Pan, José Luis Cabellos, Wei-yan Liang, Zhong-hua Cui, and Gabriel Merino. Li<sub>2</sub>B<sub>12</sub> and Li<sub>3</sub>B<sub>12</sub>: Prediction of the smallest tubular and cage-like boron structures. *Angewandte Chemie International Edition*, 57(17):4627–4631, 2018.
- <sup>75</sup> Jin-Chang Guo, Lin-Yan Feng, Ying-Jin Wang, Said Jalife, Alejandro Vásquez-Espinal, Jose Luis Cabellos, Sudip Pan, Gabriel Merino, and Hua-Jin Zhai. Coaxial triple-layered versus helical Be<sub>6</sub>B<sub>11</sub><sup>−</sup> clusters: Dual structural fluxionality and multifold aromaticity. *Angewandte*

- Chemie International Edition*, 56(34):10174–10177, 2017.
- <sup>76</sup> Xue Dong, Said Jalife, Alejandro Vásquez-Espinal, Jorge Barroso, Mesías Orozco-Ic, Estefanía Ravell, Jose Luis Cabellos, Wei-yan Liang, Zhong-hua Cui, and Gabriel Merino.  $\text{Li}_2\text{B}_{24}$ : the simplest combination for a three-ring boron tube. *Nanoscale*, 11:2143–2147, 2019.
- <sup>77</sup> Anastassia N. Alexandrova and Alexander I. Boldyrev. Search for the  $\text{Li}_n\text{O}^{+1/-1}$  ( $n = 5-7$ ) lowest-energy structures using the ab initio Gradient Embedded Genetic Algorithm (GEGA). Elucidation of the chemical bonding in the lithium clusters. *Journal of Chemical Theory and Computation*, 1(4):566–580, 2005. PMID: 26641677.
- <sup>78</sup> Jose Luis Cabellos, Filiberto Ortiz-Chi, , and Gabriel Merino. Glomos 2.0. *Cinvestav-Merida*, 1(1):1–10, 2018.
- <sup>79</sup> Gerardo Hernández-Juárez, Estefanía Ravell, Jessica Arcudia, Ximena Zarate, Zhong-hua Cui, Gabriel Merino, and Jorge Barroso. Structural effects of alkali-metals on the  $\text{B}_{12}$  skeleton. *Phys. Chem. Chem. Phys.*, 22:17344–17350, 2020.
- <sup>80</sup> Dmitry Yu. Zubarev and Alexander I. Boldyrev. ”developing paradigms of chemical bonding: adaptive natural density partitioning. *Phys. Chem. Chem. Phys.*, 10:5207–5217, 2008.
- <sup>81</sup> Zhen Hua Li, Ahren W. Jasper, and Donald G. Truhlar. Structures, rugged energetic landscapes, and nanothermodynamics of  $\text{Al}_n$  ( $2 \leq n \leq 65$ ) particles. *Journal of the American Chemical Society*, 129(48):14899–14910, 2007. PMID: 17994736.
- <sup>82</sup> Eugenia Dzib, Jose Luis Cabellos, Filiberto Ortíz-Chi, Sudip Pan, Annia Galano, and Gabriel Merino. Eyringpy: A program for computing rate constants in the gas phase and in solution. *International Journal of Quantum Chemistry*, 119(2):e25686, 2019.
- <sup>83</sup> Zhen Hua Li and Donald G. Truhlar. Nanothermodynamics of metal nanoparticles. *Chem. Sci.*, 5:2605–2624, 2014.
- <sup>84</sup> Stefan Grimme. Supramolecular binding thermodynamics by dispersion-corrected density functional theory. *Chemistry - A European Journal*, 18(32):9955–9964, 2012.
- <sup>85</sup> Philipp Pracht and Stefan Grimme. Calculation of absolute molecular entropies and heat capacities made simple. *Chem. Sci.*, 12:6551–6568, 2021.
- <sup>86</sup> D.A. McQuarrie and M.Q.D. A. *Statistical Mechanics*. Chemistry Series. Harper & Row, 1975.
- <sup>87</sup> T.L. Hill. *An Introduction to Statistical Thermodynamics*. Addison-Wesley series in chemistry. Dover Publications, 1986.
- <sup>88</sup> Ana María Mendoza-Wilson, René Renato Balandrán-Quintana, and José Luis Cabellos. Thermochemical behavior of sorghum procyanidin trimers with  $\text{C}_4$ - $\text{C}_8$  and  $\text{C}_4$ - $\text{C}_6$  interflavan bonds in the reaction with superoxide anion radical and  $\text{H}_2\text{O}_2$ -forming NADH-oxidase flavoenzyme. *Computational and Theoretical Chemistry*, 1186:112912, 2020.
- <sup>89</sup> Peter L. Rodriguez-Kessler, Adan R. Rodriguez-Dominguez, and Alvaro Muñoz Castro. Systematic cluster growth: a structure search method for transition metal clusters. *Phys. Chem. Chem. Phys.*, 23:4935–4943, 2021.
- <sup>90</sup> Dil K. Limbu, Michael U. Madueke, Raymond Atta-Fynn, David A. Drabold, and Parthapratim Biswas. Ab initio density-functional studies of 13-atom Cu and Ag clusters. *Journal of Physics: Conference Series*, 1252:012009, jun 2019.
- <sup>91</sup> Galip H. Guvelioglu, Pingping Ma, Xiaoyi He, Robert C. Forrey, and Hansong Cheng. First principles studies on the growth of small Cu clusters and the dissociative chemisorption of  $\text{H}_2$ . *Phys. Rev. B*, 73:155436, Apr 2006.
- <sup>92</sup> Mukul Kabir, Abhijit Mookerjee, and A. Bhattacharya. Copper clusters: electronic effect dominates over geometric effect. *The European Physical Journal D - Atomic, Molecular, Optical and Plasma Physics*, 31(3):477–485, December 2004.
- <sup>93</sup> Linus Pauling. On the nature of the bonding in  $\text{Cu}_2$  a comment. *The Journal of Chemical Physics*, 78(6):3346–3346, 1983.
- <sup>94</sup> Takeshi Iwasa, Takaaki Sato, Makito Takagi, Min Gao, Andrey Lyalin, Masato Kobayashi, Ken-ichi Shimizu, Satoshi Maeda, and Tetsuya Taketsugu. Combined automated reaction pathway searches and sparse modeling analysis for catalytic properties of lowest energy twins of  $\text{Cu}_{13}$ . *The Journal of Physical Chemistry A*, 123(1):210–217, 2019.
- <sup>95</sup> R. C. Longo and L. J. Gallego. Structures of 13-atom clusters of FCC transition metals by ab initio and semiempirical calculations. *Phys. Rev. B*, 74:193409, Nov 2006.
- <sup>96</sup> E. de la Puente, A. Aguado, A. Ayuela, and J. M. López. Structural and electronic properties of small neutral  $(\text{MgO})_n$  clusters. *Phys. Rev. B*, 56:7607–7614, Sep 1997.
- <sup>97</sup> Jianmin Tao, John P. Perdew, Viktor N. Staroverov, and Gustavo E. Scuseria. Climbing the density functional ladder: Nonempirical meta-generalized gradient approximation designed for molecules and solids. *Phys. Rev. Lett.*, 91:146401, Sep 2003.
- <sup>98</sup> John P. Perdew, Kieron Burke, and Matthias Ernzerhof. Generalized gradient approximation made simple. *Phys. Rev. Lett.*, 77(18):3865–3868, October 1996.
- <sup>99</sup> Timothy J. Lee and Peter R. Taylor. A diagnostic for determining the quality of single-reference electron correlation methods. *International Journal of Quantum Chemistry*, 36(S23):199–207, 1989.
- <sup>100</sup> Antonio Fernández-Ramos, Benjamin A. Ellingson, Rubén Meana-Pañeda, Jorge M. C. Marques, and Donald G. Truhlar. Symmetry numbers and chemical reaction rates. *Theoretical Chemistry Accounts*, 118(4):813–826, Oct 2007.
- <sup>101</sup> Michael K. Gilson and Karl K. Irikura. Symmetry numbers for rigid, flexible, and fluxional molecules: Theory and applications. *The Journal of Physical Chemistry B*, 114(49):16304–16317, 2010. PMID: 21141931.
- <sup>102</sup> Valeri G. Grigoryan and Michael Springborg. Temperature and isomeric effects in nanoclusters. *Phys. Chem. Chem. Phys.*, 21:5646–5654, 2019.
- <sup>103</sup> Prince Ravat. Carbo[n]helicenes restricted to enantiomerize: An insight into the design process of configurationally stable functional chiral PAHs. *Chemistry - A European Journal*, 27(12):3957–3967, 2021.
- <sup>104</sup> Bjorn Jensen. Quantum mechanics on surfaces. In Mohammad Reza Pahlavani, editor, *Some Applications of Quantum Mechanics*, chapter 8. IntechOpen, Rijeka, 2012.

## Appendix A: Boltzmann Probabilities computed at TPSS/def2-TZVP PBE/def2-TZVP PB68/def2-TZVP

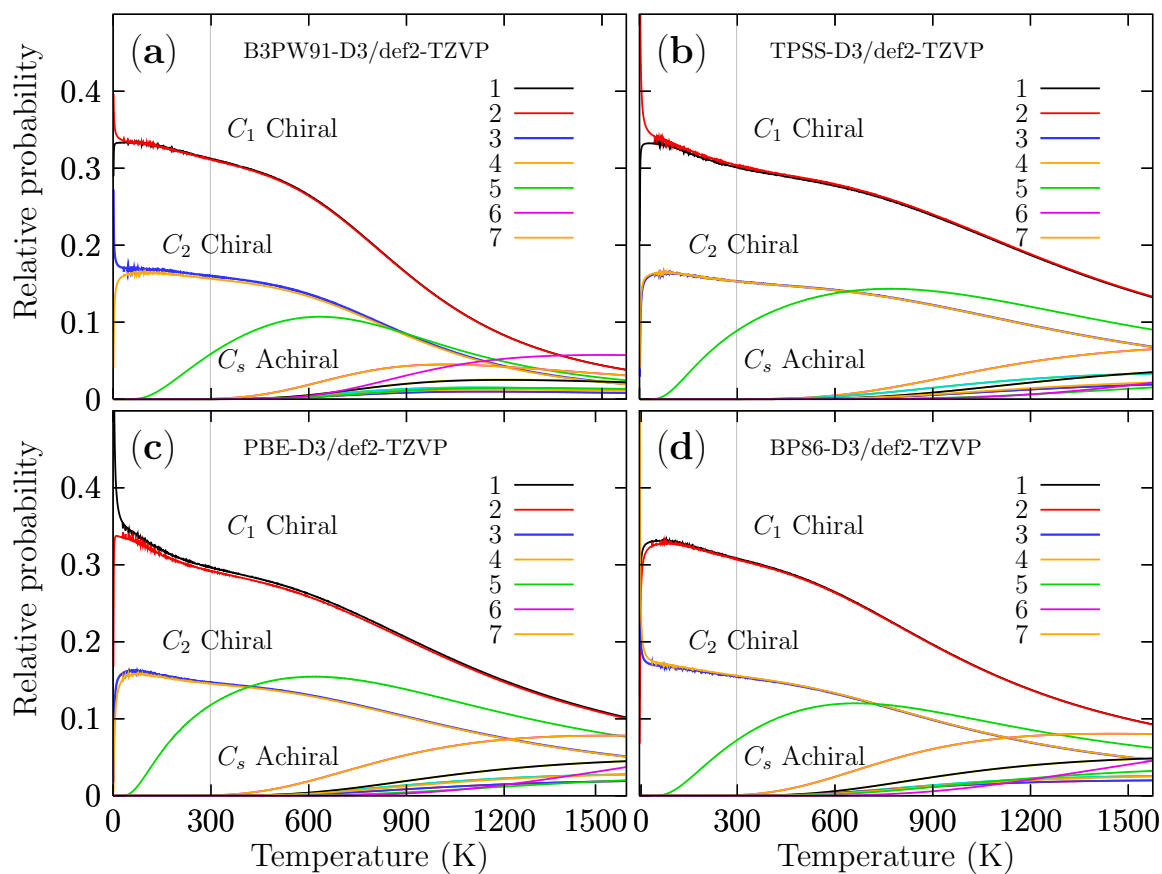


FIG. 6: (Color online) Probability of occurrence for all isomers at temperatures ranging from 20 to 1500 K computed with DFT functionals: TPSS, PBE, and BP86. The bulk melting temperature of copper is 1358 K<sup>102</sup>; thus, our results below this temperature are consistent.

## Appendix B: XYZ atomic coordiantes

```
13
0.0
Cu -0.990009000000  0.202990000000  0.910273000000
Cu  0.989148000000  0.203204000000 -0.910494000000
Cu  1.307754000000  0.817211000000  1.506707000000
Cu -0.756524000000 -1.521352000000 -1.012184000000
Cu -2.995439000000 -0.494575000000 -0.267184000000
Cu -0.000551000000  2.308713000000 -0.000120000000
Cu  1.705678000000 -2.128579000000 -1.124758000000
Cu  2.995766000000 -0.493776000000  0.267529000000
Cu  0.756822000000 -1.521006000000  1.012214000000
Cu -1.308834000000  0.816218000000 -1.506262000000
Cu -1.705107000000 -2.129263000000  1.124856000000
Cu  2.516484000000  1.969366000000 -0.285914000000
Cu -2.515188000000  1.970848000000  0.285338000000
13
0.0
Cu  0.000000000000  1.344973000000  0.202955000000
Cu  0.000000000000 -1.344973000000  0.202955000000
Cu -1.995454000000  0.058043000000  0.817297000000
Cu  1.256550000000 -0.129438000000 -1.520715000000
Cu  2.225189000000  2.023127000000 -0.494441000000
Cu  0.000000000000  0.000000000000  2.309851000000
Cu -0.329078000000 -2.016616000000 -2.128802000000
Cu -2.225189000000 -2.023127000000 -0.494441000000
Cu -1.256550000000  0.129438000000 -1.520715000000
Cu  1.995454000000 -0.058043000000  0.817297000000
Cu  0.329078000000  2.016616000000 -2.128802000000
Cu -1.493610000000 -2.046117000000  1.968780000000
Cu  1.493610000000  2.046117000000  1.968780000000
```